Cockcroft-09-29

MODIFICATION OF THE EMMA INJECTION LINE TO ACT AS A FULL-ENERGY ELECTRON BEAM DIAGNOSTIC FOR ALICE

D.J.Holder, Liverpool University and Cockcroft Institute, UK

MODIFICATION OF THE EMMA INJECTION LINE TO ACT AS A FULL-ENERGY ELECTRON BEAM DIAGNOSTIC FOR ALICE

D.J.Holder, Liverpool University and Cockcroft Institute, UK.

INTRODUCTION

ALICE (Accelerators and Lasers in Combined Experiments) experimental facility (known formerly as ERLP) is being commissioned at present. It is based on a combination of a DC photocathode electron gun, a superconducting injector linac and a main linac operating in energy recovery mode. These drive an infrared Free-Electron Laser (IR-FEL) an inverse Compton Back-Scattering (CBS) x-ray source and a terahertz beamline. Originally conceived as a prototype test-bed for the key concepts and technologies expected to feature in the UK's next major light source project, the 4th Generation Light Source (4GLS), it now has a broader role as an accelerator physics and technology test facility and to develop fourth generation light source science. The nominal parameters for ALICE are shown in table 1.

Table 1: Nominal ALICE parameters

Nominal gun energy	**350**	keV
Injector energy	**8.35**	MeV
Circulating beam energy	**35**	MeV
RF frequency	**1.3**	GHz
Bunch repetition rate	**81.25**	MHz
Nominal bunch charge	**80**	pC
Maximum train length	**100**	μs
Maximum train repetition rate	**20**	Hz
Maximum average current	**13**	μA

ALICE will also act as an injector for what will be the world's first non-scaling, Fixed-Field Alternating Gradient (FFAG) accelerator called EMMA (Electron Machine with Many Applications). FFAGs similar to EMMA have an unprecedented potential for medical accelerators for carbon and proton hadron therapy. It is also a contender for the active element for an ADSR (Accelerator Driven Sub-critical Reactor).

When ALICE is operating as an injector for EMMA, it will be at a reduced energy of 10 to 20 MeV, compared to its nominal energy of 35 MeV. Therefore an injection line has been designed, consisting of a dogleg to extract the beam from ALICE, a matching section, a tomography section and some additional dipoles and quadrupoles, to transport and match the beam to the entrance of EMMA. This injection line was designed both to transport the beam from ALICE to EMMA and act as a diagnostic to measure as fully as possible the properties of the beam being injected into EMMA, *in the expected energy range of 10 to 20 MeV*. However, it occurred to me that this injection line could act as a very useful diagnostic tool for ALICE operation, enabling the measurement of ALICE beam properties, if it could be modified to operate at an energy of 35 MeV. In addition to being designed to operate at maximum energy of 20 MeV, the injection line was also intended to operate with a bunch charge of up to 32 pC. The project described in this report

consists of three stages undertaken by me; firstly an assessment as to whether this modification was technically (and financially) viable, secondly a calculation of the changes required and thirdly a calculation of the magnet settings required for the successful propagation of the electron beam down the modified line.

Figure 1 shows the layout of both ALICE and EMMA with the injection and extraction lines.

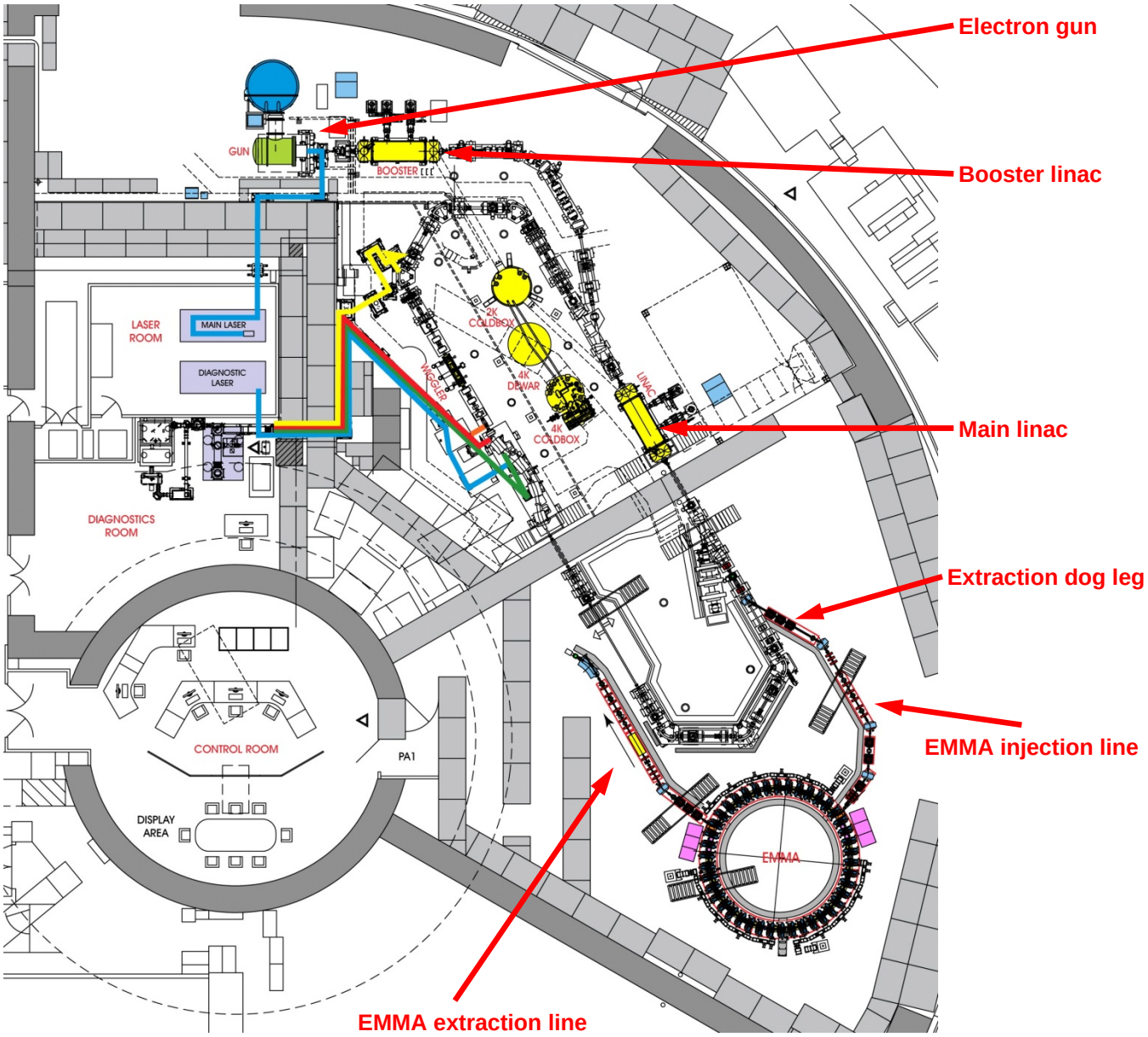

Figure 1: Layout of ALICE & EMMA

CURRENT STATUS

ALICE: The nominal gun operating voltage of 350 kV was achieved initially during gun commissioning [1] but, after several failures of the high voltage insulating ceramics, it was necessary to install a more robust but smaller inner diameter ceramic that has reduced the maximum gun operating voltage to ~250 kV. A problem with a field emitter on the GaAs cathode wafer, located close to its centre, has necessitated a further reduction in the gun voltage to 230 kV. In addition, high levels of field emission inside the superconducting accelerating modules, particularly the main linac, has restricted the maximum operating energy. In order to maintain the correct ratio of injection to full energy (required for the fixed geometry of the beam injection

and dump dog legs), the injector has been operated most recently at 4.8 MeV with a full energy beam of 20.8 MeV. These issues are described in more detail here [2]. The regime of 230 kV/4.8 MeV/20.8 MeV is likely to be the default operational mode now for some time, due to the long lead time and risk involved in fixing the problems with both the gun and the superconducting linac. Full energy recovery and demonstration of the coherently-enhanced terahertz radiation were successfully achieved towards the end of 2008 and the beginning of 2009.

EMMA: Construction of EMMA commenced this year [3], with the installation of many of the services well underway and installation of the girder modules that form most of the injection line already completed, shown in figure 2. The EMMA injection line is expected to be ready in the later part of 2009, the first part of EMMA to be finished. This is a happy coincidence as this is also the time at which the first attempts will be made to operate ALICE's FEL, for which precise knowledge of the beam properties will be crucial.

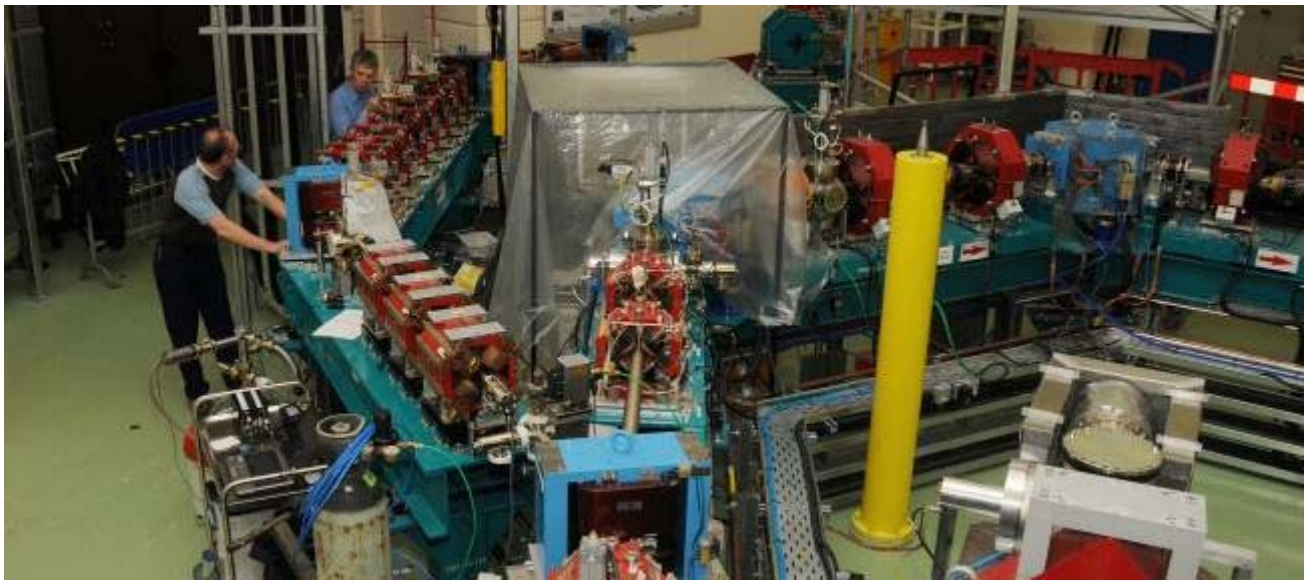

Figure 2: EMMA injection line modules being installed.

INJECTION LINE DESIGN

The EMMA injection line consists of a symmetric 30° dog leg (a combination of two dipoles and (usually) a number intermediate quadrupoles that produce a lateral displacement of the beam), the first dipole extracting the beam from ALICE followed by three quadrupoles and second dipole. This is then followed by a matching and tomography section and last dispersive section, as is shown in figure 3. The purpose of the dog leg is to set zero dispersion (the variation of trajectory with beam energy), before the beam enters a matching section followed by the tomography section. The matching section ensures that the correct beam properties are obtained at the entrance of the tomography section. The tomography section is a beam diagnostic that allows the transverse phase space of the beam to be measured. When the EMMA injection line was designed, the intention was that it would be used to fully characterise the beam before its injection into EMMA. This project investigates the extension of the functionality of this line to measure the beam properties at the full ALICE energy of 35 MeV

After the tomography section there is a further dispersive section before the EMMA ring (including a number of diagnostic instruments) but it is not intended that this is used for ALICE beam measurements; a rather convenient dipole and Faraday cup/beam dump follows the tomography section allowing the ALICE beam to be dumped and its charge measured. There are also a number of horizontal and vertical steerers in the line for centring the beam. The design of the injection and extraction lines is detailed in [4].

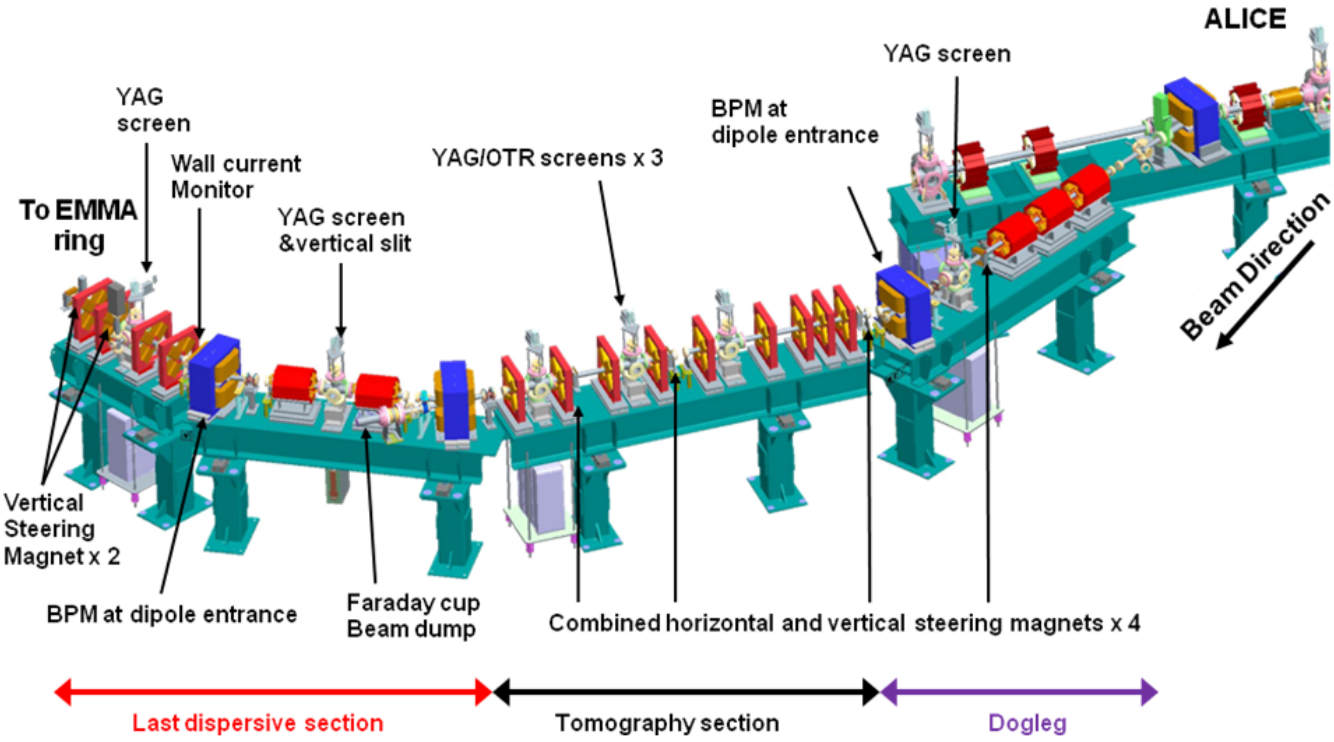

Figure 3: Layout of EMMA injection line

PHASE SPACE TOMOGRAPHY

A phase space tomography diagnostic consists of a quadrupole matching section followed by a number of FODO (horizontally-focussing quadrupole – drift space – vertically-focussing quadrupole – drift space) cells with screens around them. Due to space constraints the minimum three screen measurement was implemented. The beam is matched into the FODO lattice by quadrupoles upstream of the tomography measurement diagnostic such that the Twiss parameters that are used to characterise the propagating beam (particularly the alpha and beta functions) are well defined at its entrance. For a measurement at a particular energy the field strength in the FODO quadrupoles remains constant and their gradient alternates in sign. In addition the screen-to-screen phase advance is set to 60° (the optimum is 180°/n, where n is the number of screens). Images of the beam on the Optical Transition Radiation (OTR) screens are at different orientations in phase space and thus with knowledge of the phase advance between FODO cells the phase space of the beam can be re-constructed. Knowledge of the beta functions then allows an emittance measurement to be inferred from the area of phase space measured.

INJECTION LINE HARDWARE MODIFICATIONS

In order to determine whether this proposal was economically viable, it was critical to determine whether the existing magnet designs were likely to be adequate for operation at 35 MeV, as changes to these magnets would not be possible. It was also necessary to calculate whether the magnet power supplies already specified (but fortunately not already installed) would be capable of providing the additional current likely to be required. Table 2 shows the original magnet and power supply calculations for 20 MeV (based on the nominal field strength specification) and rescaled values for 35 MeV. The full set of magnet parameters are in appendices 1 and 2.

Table 2: Nominal 20 MeV magnet parameters rescaled for 35 MeV (the full table of magnet parameters can be found in appendix 1)

Magnet type		Nominal values					
		K1 (m^{-2})	Gradient (T/m)	Field (T)	Voltage (V)	Current (A)	Current density (A/mm^2)
					20 MeV		
F	dipole		-	0.173	16.8	6.0	0.8
G	dipole		-	0.190	14.0	5.3	0.7
G	quadrupole	20	1.4	-	1.0	66	
H	quadrupole	124	8.5	-	8.5	5.6	1.4
					35 MeV		
F	dipole		-	0.303	**29.4**	**10.5**	1.4
G	dipole		-	0.333	**24.4**	**9.3**	1.2
G	quadrupole	20	2.4	-	1.7	**115**	
H	quadrupole	124	14.7	-	14.9	9.9	2.5
				Power supply:	**Rating**		**Max current**
					(V)	(A)	(A)
F	dipole		Needs up-rating		20	10	6.7
G	dipole		Needs up-rating		20	10	6.7
G	quadrupole		Needs up-rating				66
H	quadrupole		OK		20	10	9.9

It is apparent in the table that both the field for the dipole magnets and the current density for the quadrupole magnets are within reasonable engineering limits, and therefore can be expected to operate without modification at the higher energy. However, it can also be seen that three out of the four types of magnet power supplies originally specified will not provide sufficient output and have had to be replaced with ones with a higher rating. Note that this calculation has been done with the nominal magnet fields, i.e. not taking into account the actual values required when the electron beam was matched from ALICE to EMMA. In fact the calculated quadrupole field gradients required (for the original 20 MeV design) were significantly less than these nominal values. However it is prudent at this stage to work with these figures and use them as an upper constraint for any matching done for 35 MeV, due to the long timescale involved in specifying and installing power supplies.

In addition to the up-rating of the magnet power supplies OTR screens have been added in parallel with the original YAG screens in the tomography section of the EMMA injection line, as they are more suitable for use at the higher energy.

CALCULATION OF NEW QUADRUPOLE SETTINGS

The quadrupole strengths calculated for the injection line to match a beam from ALICE (operating at 10 to 20 MeV) into the tomography section will not be correct for a number of reasons:

- The beta functions at the exit point of ALICE will vary as a function of beam energy due to RF focussing in the linac modules and different quadrupole settings in ALICE to deal with space charge defocusing of the beam;
- No account has been taken so far to compensate for the effect of space charge in the injection line itself. For the higher nominal bunch charge of 80 pC for ALICE the effect of space charge may be more significant, although the higher energy may mitigate this to some extent.

The new quadrupole settings for the EMMA injection line, used as a diagnostic for ALICE at 35 MeV and 80 pC, are first calculated using the tracking code MAD8. With this code it is possible to take a beam with a particular set of Twiss parameters and not only calculate their evolution along a beam line but also require them to attain a certain value at the end of the beam line (a process called matching).

However, this code does not calculate the effect of space charge, where the mutually repulsive forces between the electrons in the beam result in an overall defocusing force leading to emittance growth and a mis-matching. A procedure to overcome this is described here [5], which uses the code General Particle Tracer (GPT) [6] to calculate the forces between the charges in the beam as the beam propagates and then includes this force in the beam propagation calculation.

SPACE CHARGE

If one considers a beam passing through a drift space (i.e. in the absence of external focussing forces) the mutual repulsion of every electron from those around can be modelled as a quadrupole defocusing force in both the *x* and *y* planes. This phenomenon is called space charge and is a particular problem for low energy and/or high charge density beams. It leads to a growth in beam size and limits the performance of sources of high-brightness (i.e. high charge density) electrons, which are much sought after for synchrotron light sources and high energy physics accelerators. Once the electron beam has attained a velocity close to the speed of light (often described as being relativistic) then the increased rigidity of the beam (a measure of its resistance to being manipulated with a magnetic field) means that the defocusing effect of space charge becomes insignificant.

Considering a beam coasting in the z direction (so that it has no properties directly dependent on this coordinate), then in cylindrical coordinates (r, θ, z) the electric and magnetic fields can be written as:

$$E_r = \frac{4\pi}{r}\int_0^r \rho(r')\, r' dr'$$

$$B_\theta = \frac{v}{c}\frac{4\pi}{r}\int_0^r \rho(r')\, r' dr'$$

Where $\rho(r)$ is the charge density $(r^2 = x^2 + y^2)$ and all particles are been assumed to be travelling in the z direction with velocity v and where c is the speed of light. This means that the Lorentz force has only a radial component, given by:

$$F_r = eE_r - e\beta B_\theta = \frac{1}{\gamma^2} eE_r$$

where $\beta = \frac{v}{c}$ and $\gamma = \frac{1}{\sqrt[2]{(1-\beta^2)}}$ have their normal relativistic meaning.

For an elliptical cross-section beam with current I:

$$\rho(x, y) = \frac{I}{v\pi ab}\phi\left(1 - \frac{x^2}{a^2} - \frac{y^2}{b^2}\right)$$

where ϕ is a step function with $\phi(t) = 1$ if $t \geq 0$ and 0 otherwise. The electric field inside the beam (i.e. for $\frac{x^2}{a^2} + \frac{y^2}{b^2} < 1$) is given by:

$$E_x(x, y) = \frac{4I}{v}\frac{x}{a(a+b)}$$

$$E_y(x,y) = \frac{4I}{v}\frac{y}{b(a+b)}$$

from which the Lorentz force can be seen to be:

$$F_x(x,y) = \frac{4eI}{v\gamma^2}\frac{x}{a(a+b)}$$

$$F_y(x,y) = \frac{4eI}{v\gamma^2}\frac{y}{b(a+b)}$$

For a round beam, the equation of transverse motion of a particle in the beam has the form:

$$\gamma m\frac{d^2r}{dt^2} = \frac{2eI}{\gamma^2 v a^2}r$$

using the paraxial approximation $\left(\left|\frac{dr}{dt}\right| \ll v\right)$. If the initial particle velocities depend linearly on the initial coordinates then their trajectories do not cross and the beam is laminar. In this case, this equation is also true for boundary particles $(r = a)$. Therefore, putting $z = vt$ into this equation it becomes:

$$\frac{d^2a}{dz^2} = \frac{2I}{(\beta\gamma)^3 I_0}\frac{1}{a}$$

$I_0 = \frac{4\pi\varepsilon_0 mc^3}{e}$ is known as the Alfvén current and is approximately equal to 17 kA for electrons. If linear external focusing is also added, the equation becomes:

$$\frac{d^2a}{dz^2} + K(z)a - \frac{2I}{(\beta\gamma)^3 I_0}\frac{1}{a} = 0$$

where $K(z)$ is the focusing rigidity. For a focusing lens at $z = 0$, $K(z) = \frac{\delta(z)}{F}$, where $\delta(z)$ is the normal delta function and F is the focal strength.

If, for simplicity, we consider a uniform elliptical beam, with a distribution given by the Kapchinsky-Vladimirsky (KV) function, it is possible to describe the evolution of the beam with envelope equations (known as the Kapchinsky-Vladimirsky equations). From these one can calculate the transverse equations of motion in the presence of space charge and external focusing, and as long as the external focussing is smaller than the effect of space charge (which ensures that the beam remains laminar) then the growth in effective emittance (for the KV distribution, the rms emittance is related to the effective emittance by $\varepsilon^{rms} = \frac{\varepsilon_x}{4}$) can be calculated.

For a round pencil-like beam of peak current I_{max} passing through a drift of length L, the emittance increase due to space charge is:

$$\Delta\varepsilon_x \cong \frac{0.14 I_{max} L}{(\beta\gamma)^3 I_0}$$

which is independent of the transverse beam size. However, non-linearities have not been included in this calculation and for real (non-KV) distributions, the factor 0.14 becomes nearer to 0.2.

MODELLING IN MAD8

The first step (ignoring space charge) is to use MAD8 with Twiss parameters at the exit of the booster linac derived from ASTRA modelling of the injector [7] to transport the beam as far as the new dipole magnet that extracts the beam into the EMMA injection line, using the standard ALICE lattice tuning (known as 8.5). After extraction, MAD8 is used to match the beam into the tomography diagnostic, giving the Twiss parameters required at this point from the existing tomography section design, by finding new settings for the EMMA injection line quadrupoles. The constraints employed are:

- Standard ALICE lattice 8.5 tuning from the exit of the booster module to the new extraction dipole;
- Zero dispersion in the extraction dog leg;
- Beta functions between main linac and start of the matching section <20 m;
- Matched to specific Twiss parameters at the first screen of the tomography diagnostic;
- Quadrupole gradients must not exceed the limit set by the new magnet power supplies.

Table 3 shows the values of the Twiss parameters at the exit of the ALICE booster linac (i.e. the starting conditions) and at the first screen the tomography diagnostic (i.e. the finishing conditions) while table 4 lists the elements that make up the whole line modelled in MAD8; i.e. a combination of ALICE from the exit of the booster linac to the end of the tomography diagnostic in the EMMA injection line.

Table 3: Start and end Twiss parameters used for MAD modelling

	α_x	α_y	β_x	β_y
			(m)	(m)
ALICE booster exit	-2.2	-2.2	13.4	13.4
Tomography section entrance	-1.235	1.235	0.7439	0.7439

Table 4: The elements included in the beam line modelled in MAD8

Element		**Elapsed distance**	**Description**	**Comment**
name	**length**			
	(m)	(m)		
PREINJM	0	0	Marker	Marks the end of booster linac
INJDRIFT01	0.09	0.09	Drift	
INJQUAD01	0.15	0.24	Quadrupole	Not varied – set to ALICE lattice 8.5 value
INJDRIFT02	0.45	0.69	Drift	
INJQUAD02	0.15	0.84	Quadrupole	Not varied – set to ALICE lattice 8.5 value
INJDRIFT03	0.5321	1.3721	Drift	
INJQUAD03	0.15	1.5221	Quadrupole	Not varied – set to ALICE lattice 8.5 value
INJDRIFT04	0.3	1.8221	Drift	
INJQUAD04	0.15	1.9721	Quadrupole	Not varied – set to ALICE lattice 8.5 value
INJDRIFT05	0.5	2.4721	Drift	
INJDIPOLE01	0.2	2.6721	Sector dipole	
INJDRIFT06	0.4	3.0721	Drift	
INJQUAD05	0.15	3.2221	Quadrupole	Not varied – set to ALICE lattice 8.5 value
INJDRIFT07	0.4	3.6221	Drift	
INJDIPOLE02	0.2	3.8221	Sector dipole	
INJDRIFT08	0.695	4.5171	Drift	
INJQUAD06	0.15	4.6671	Quadrupole	Not varied – set to ALICE lattice 8.5 value

INJDRIFT09	0.25	4.9171	Drift	
INJQUAD07	0.15	5.0671	Quadrupole	Not varied – set to ALICE lattice 8.5 value
INJDRIFT10	0.25	5.3171	Drift	
INJQUAD08	0.15	5.4671	Quadrupole	Not varied – set to ALICE lattice 8.5 value
INJDRIFT11	0.25	5.7171	Drift	
INJQUAD09	0.15	5.8671	Quadrupole	Not varied – set to ALICE lattice 8.5 value
INJDRIFT12	0.25	6.1171	Drift	
XD	0.0075	6.1246	Drift	
INJDIPOLE03	0.2	6.3246	Sector dipole	
XD4	0.001875	6.326475	Drift	
INJDRIFT13	1	7.326475	Drift	
INJQUAD10	0.15	7.476475	Quadrupole	Not varied – set to ALICE lattice 8.5 value
XD4	0.001875	7.47835	Drift	
INJDRIFT14	1	8.47835	Drift	
INJQUAD11	0.15	8.62835	Quadrupole	Not varied – set to ALICE lattice 8.5 value
XD4	0.001875	8.630225	Drift	
INJDRIFT15	1	9.630225	Drift	
INJQUAD12	0.15	9.780225	Quadrupole	Not varied – set to ALICE lattice 8.5 value
XD4	0.001875	9.7821	Drift	
INJDRIFT16	1	10.7821	Drift	
ST4DIP03LOW	0.215	10.9971	Sector dipole	
ST1DRIFT01	1.397	12.3941	Drift	
TENDDRIFT	0.44	12.8341	Drift	
TCAVITY1A	1.0362	13.8703	Linac cavity	
TINTDRIFT	0.3126	14.1829	Drift	
TCAVITY2A	1.0362	15.2191	Linac cavity	
TENDDRIFT	0.44	15.6591	Drift	
ST1DRIFT02	2.5087	18.1678	Drift	
ST1DIP01HIGH	0.215	18.3828	Sector dipole	
ST1DRIFT03	0.457	18.8398	Drift	
ST1DIP02	0.43	19.2698	Sector dipole	
ST1DRIFT04	0.457	19.7268	Drift	
ST1DIP03	0.215	19.9418	Sector dipole	
ST1DRIFT05	0.296	20.2378	Drift	
ST1QUAD01	0.1524	20.3902	Quadrupole	**Varied to get β_x & β_y < 20 m from main linac to start of matching section**
ST1DRIFT06	0.8776	21.2678	Drift	
ST1QUAD02	0.1524	21.4202	Quadrupole	**Varied to get β_x & β_y < 20 m from main linac to start of matching section**
ST1DRIFT07	0.258	21.6782	Drift	
ALICEND	0	21.6782	Marker	**Marks the end of ALICE**
ST1DIP04	**0.2**	**21.8782**	**Sector dipole**	**First magnet of extraction dog leg**
EMIDRIFT01	0.828	22.7062	Drift	
EMIQUAD01	0.275	22.9812	Quadrupole	**Varied to get zero D_x and D_x' at the end of dog leg**

EMIDRIFT02	0.146	23.1272	Drift	
EMIQUAD02	0.275	23.4022	Quadrupole	**Fixed while matching dog leg, then varied to get β_x & β_y < 20 m from main linac to start of matching section, before dog leg matching repeated**
EMIDRIFT03	0.146	23.5482	Drift	
EMIQUAD03	0.275	23.8232	Quadrupole	**Varied to get zero Dx and Dx' at the end of dog leg**
EMIDRIFT04	0.828	24.6512	Drift	
EMIDIP01	**0.2**	**24.8512**	**Sector dipole**	**Last magnet of extraction dog leg**
EMIDRIFT05	0.336	25.1872	Drift	
EMIQUAD04	0.07	25.2572	Quadrupole	**Varied to match into tomography section**
EMIDRIFT06	0.1	25.3572	Drift	
EMIQUAD05	0.07	25.4272	Quadrupole	**Varied to match into tomography section**
EMIDRIFT07	0.1	25.5272	Drift	
EMIQUAD06	0.07	25.5972	Quadrupole	**Varied to match into tomography section**
EMIDRIFT08	0.219	25.8162	Drift	
EMIQUAD07	0.07	25.8862	Quadrupole	**Varied to match into tomography section**
EMID09	0.3035	26.1897	Drift	
TSTART	0	26.1897	Marker	
SCREEN	**0**	**26.1897**	**Marker**	**First screen of tomography diagnostic**
L2	0.1475	26.3372	Drift	
QT1	0.07	26.4072	Quadrupole	Not varied – set by tomography section design
L1	0.295	26.7022	Drift	
QT2	0.07	26.7722	Quadrupole	Not varied – set by tomography section design
L2	0.1475	26.9197	Drift	
SCREEN	**0**	**26.9197**	**Marker**	**Second screen of tomography diagnostic**
L2	0.1475	27.0672	Drift	
QT1	0.07	27.1372	Quadrupole	Not varied – set by tomography section design
L1	0.295	27.4322	Drift	
QT2	0.07	27.5022	Quadrupole	Not varied – set by tomography section design
L2	0.1475	27.6497	Drift	
SCREEN	**0**	**27.6497**	**Marker**	**Final screen of tomography diagnostic**
TEND	0	27.6497	Marker	
EMID13	0.1475	27.7972	Drift	

It can be seen that in order to satisfy some of the constraints listed it was necessary to adjust the settings of the last two quadrupoles in ALICE before extraction. Figure 4 shows the beta functions obtained in both planes, starting at the exit of the ALICE booster linac up to the end of the tomography section, while figure 5 is an expansion of the tomography section only. Table 5 shows the quadrupole strengths determined by MAD8 in this simulation, which can be seen to be comfortably within the revised limits set by the new power supplies specified from the calculations in table, except for EMIQUAD07, which is slightly above.

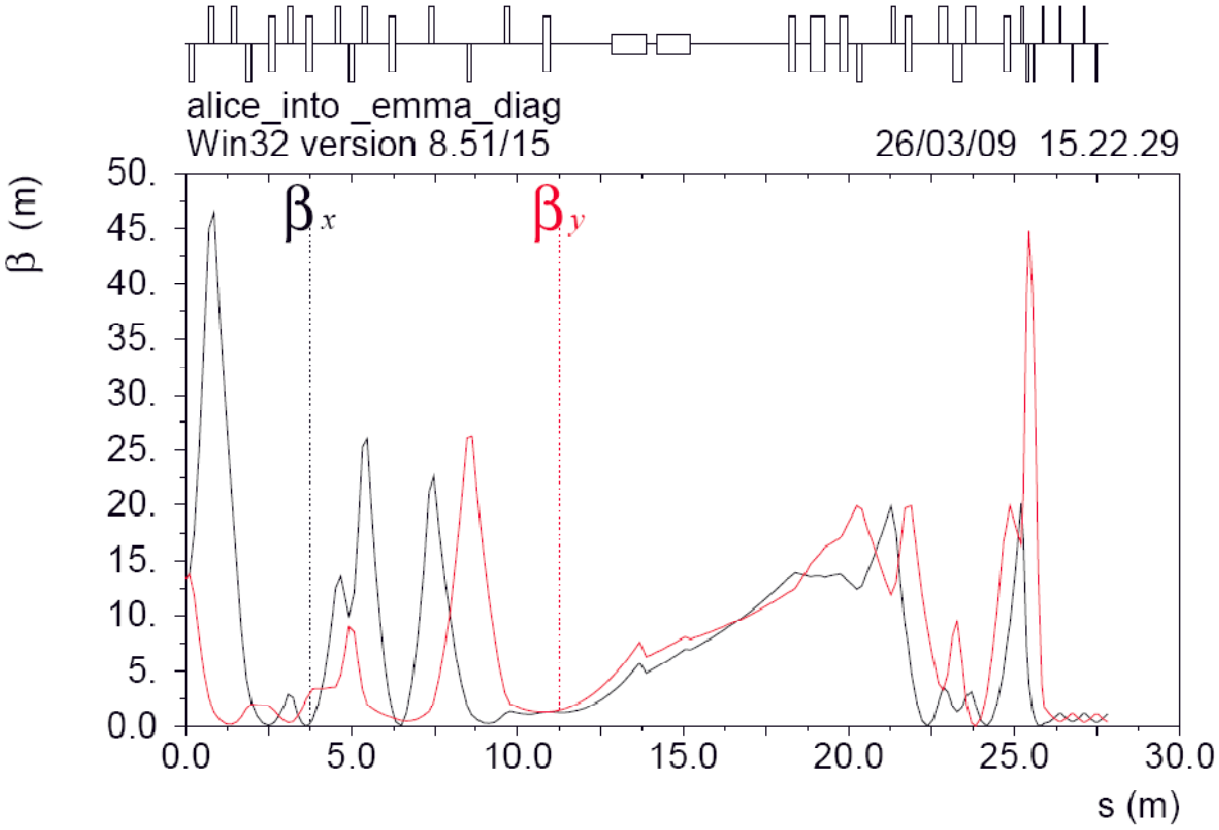

Figure 4: $\beta_{x,y}$ for the ALICE and the EMMA injection line, from the exit of the booster linac to the end of the tomography diagnostic.

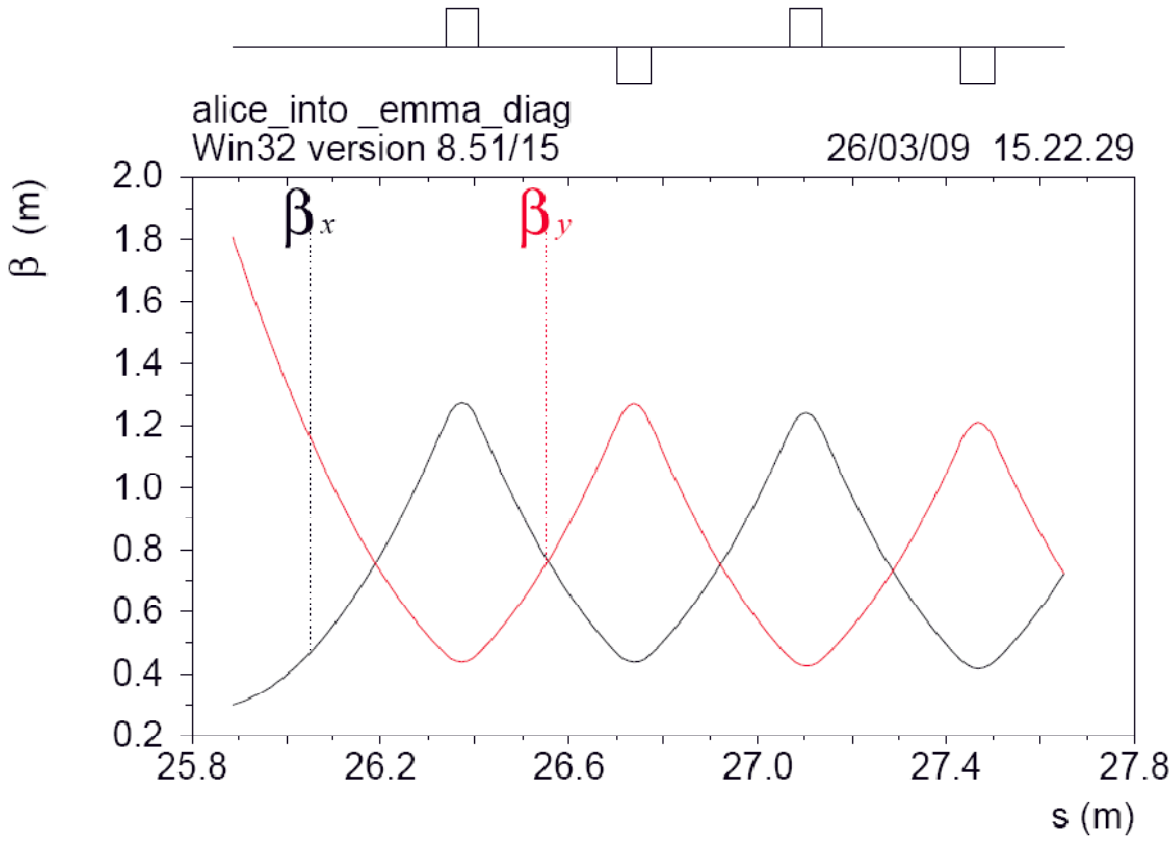

Figure 5: $\beta_{x,y}$ for the tomography section of EMMA injection line

Table 5: The calculated quadrupole strengths in the beam line when modelled in MAD8

Element name	**Quadrupole type**	**Initial value**	**MAD result**	
		K1 (m^{-2})	**K1** (m^{-2})	**Field** (T/m)
INJQUAD01		-8.6236885	**Unchanged ALICE lattice 8.5**	
INJQUAD02		9.497709		
INJQUAD03		2.6314742		
INJQUAD04		-11.773319		
INJQUAD05		25.604767		
INJQUAD06		10.911408		
INJQUAD07		-17.034718		
INJQUAD08		14.631637		
INJQUAD09		0		
INJQUAD10		11.94648196		
INJQUAD11		-8.9513017		
INJQUAD12		11.94648196		
ST1QUAD01		1.2008173	-2.63	**-0.31**
ST1QUAD02		-3.3476351	8.17	**0.97**
EMIQUAD01	**G** (2.4 T/m max)		14.48	**1.72**
EMIQUAD02	**G** (2.4 T/m max)		-14.62	**-1.73**
EMIQUAD03	**G** (2.4 T/m max)		14.48	**1.72**
EMIQUAD04	**H** (14.7 T/m max)		60.35	**7.15**
EMIQUAD05	**H** (14.7 T/m max)		-44.90	**-5.32**
EMIQUAD06	**H** (14.7 T/m max)		-29.52	**-3.50**
EMIQUAD07	**H** (14.7 T/m max)		135.43	**16.04**
QT1	**H** (14.7 T/m max)		41.92	**4.97**
QT2	**H** (14.7 T/m max)		-41.92	**-4.97**

MODELLING IN GPT

In the previous section, transport of the electron beam from the exit of the ALICE booster linac to the end of the tomography diagnostic in the EMMA injection line was simulated, excluding the effect of space charge. However, with a bunch charge of 80 pC, this may well be a significant factor than cannot be overlooked. However, an attempt can be made to compensate for the effects of space charge using the code GPT.

Previous studies [8] for the PITZ collaboration have shown that it is possible to eliminate almost entirely the mismatch induced by the defocusing effect of space charge in this situation by increasing the strength of the matching quadrupoles prior to the tomography section. In order to do this, GPT was used to model the transport of the 35 MeV beam (with 80 pC bunch charge) from the exit of the main linac (rather than from the exit of the booster linac as was used in the MAD modelling), using the beam parameters at this point derived from the MAD modelling. Table 6 shows these Twiss parameters at the exit of the main linac which are used as the starting values for the GPT modelling, along with an estimate for the normalised emittance. In [9], the most recent modelling of the ALICE injector, the normalised emittance at the booster exit has been modelled using ASTRA [10] to be 2 mm.mrad. Reference [11] estimates that the effect of space charge on a beam of this emitance would be to increase it towards 5 or 6 mm.mrad over the pathlength between the booster exit and the main linac.

Table 6: Twiss parameters at the exit of the main linac (derived from the MAD modelling) used as the starting values for the GPT modelling

α_x	α_y	β_x	β_y	**Normalised emittance**
		(m)	(m)	(mm.mrad)
-0.863	-0.553	7.644	8.333	6

The constraints employed for the GPT modelling are:

- Twiss parameters at the exit of the booster module determined by MAD result;
- No changes in the extraction dog leg (to maintain zero dispersion here);
- Matched to the same specific Twiss parameters at the first screen of the tomography diagnostic.

The elements in the GPT simulation and their function is summarised in table 7.

Table 7: The elements included in the beam line modelled in GPT

Element		**Elapsed distance**	**Description**	**Comment**
name	**length**			
	(m)	(m)		
ST1DIP01HIGH	0.215	2.7237	Sector dipole	
ST1DIP02	0.43	3.6107	Sector dipole	
ST1DIP03	0.215	4.2827	Sector dipole	
ST1QUAD01	0.1524	4.7311	Quadrupole	**Varied to match into tomography section**
ST1QUAD02	0.1524	5.7611	Quadrupole	**Varied to match into tomography section**
ST1DIP04	0.2	6.2191	Sector dipole	First magnet of extraction dog leg
EMIQUAD01	0.275	7.3221	Quadrupole	Not varied – set to MAD value
EMIQUAD02	0.275	7.7431	Quadrupole	Not varied – set to MAD value
EMIQUAD03	0.275	8.1641	Quadrupole	Not varied – set to MAD value
EMIDIP01	0.2	9.1921	Sector dipole	Last magnet of extraction dog leg
EMIQUAD04	**0.07**	**9.5981**	**Quadrupole**	**Varied to match into tomography section**
EMIQUAD05	**0.07**	**9.7681**	**Quadrupole**	**Varied to match into tomography section**
EMIQUAD06	**0.07**	**9.9381**	**Quadrupole**	**Varied to match into tomography section**
EMIQUAD07	**0.07**	**10.2271**	**Quadrupole**	**Varied to match into tomography section**
SCREEN	0	10.5306	Screen	First screen of tomography diagnostic
QT1	0.07	10.7481	Quadrupole	Not varied – set by tomography section design
QT2	0.07	11.1131	Quadrupole	Not varied – set by tomography section design
SCREEN	0	11.2606	Screen	Second screen of tomography diagnostic
QT1	0.07	11.4781	Quadrupole	Not varied – set by tomography section design
QT2	0.07	11.8431	Quadrupole	Not varied – set by tomography section design
SCREEN	0	11.9906	Screen	Final screen of tomography diagnostic

As was the case with the MAD modelling, it was again necessary to adjust the settings of the last two quadrupoles in ALICE before extraction for the correct Twiss parameters to be achieved at the first screen of the tomography section. Additionally, there are two other parameters that must be set correctly in order to for GPT to converge on a solution; these are the number of particles and the space charge model used for calculation. GPT requires the total charge in the bunch to be specified along with the number of particles. Due to the computationally intensive nature of calculating the force on every particle by every one of its neighbours, it is not practical to use a single electron as the individual element of charge. Thus for these

simulations, one thousand particles were specified; thus for the 80 pC bunch the beam consists of thousand particles with a charge 80 fC (i.e. 500,000 electrons).

GPT has five space charge models built in; each of which has a certain restricted range of applicability; for this modelling the routine "spacecharge3D" was chosen. This is a "from first principles" computationally intensive routine, calculating the interaction between all the particles in a fully relativistic manner. The computation time scales as the square of number of particles and for practical purposes this limits the number of particles to 1,000, which is not sufficient for some problems. However, it does give the most correct answer from a physics perspective.

An alternative routine, "spacecharge3Dmesh" was also experimented with. This is based on solving Poisson's equation in the rest frame of the bunch with a variable element size mesh and is the fastest routine available in GPT. It allows calculations with 1,000,000 particles on a desktop PC within a reasonable time but cannot handle a large energy spread in the bunch or near-discontinuities in the charge density distribution. In order to confirm that the solution generated by the "spacecharge3D" routine was reproducible with another calculation strategy, the modelling was repeated with the "spacecharge3Dmesh" routine, with 100, 1,000 and 10,000 particles and 80 pC. No solution was found with 100 particles, while 1,000 and 10,000 particles gave similar results to "spacecharge3D".

Initially the line was rematched in GPT using the full 3D space charge option but with zero bunch charge set, using as a starting point the quadrupole settings from the MAD. The results of this are shown in figures 6 and 7. If the bunch charge is now increased to 80 pC, without any attempt to compensate for the effect of space charge, the result seen in figure 8 is obtained; comparison with figure 6 shows the degree of mismatch induced even at 35 MeV.

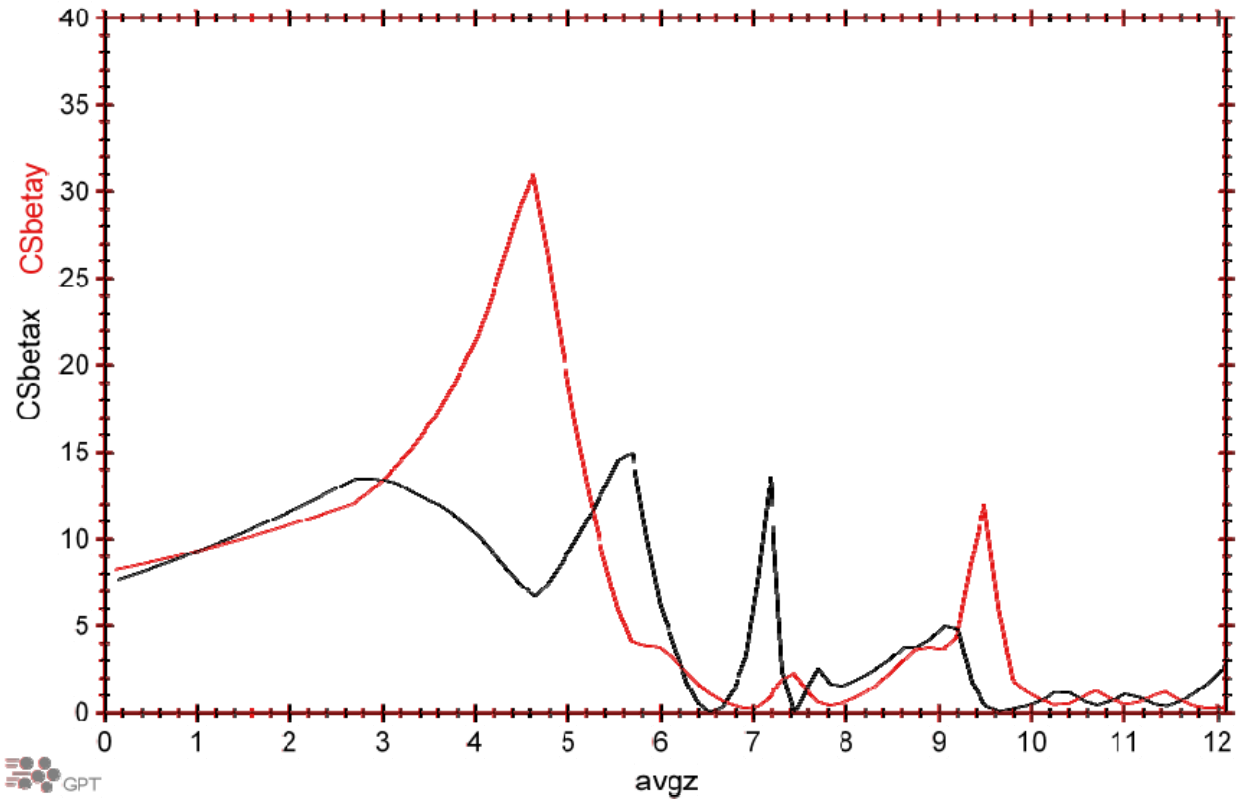

Figure 6: $\beta_{x,y}$ from the ALICE main linac exit to the end of EMMA injection line tomography section at 35 MeV and 0 pC

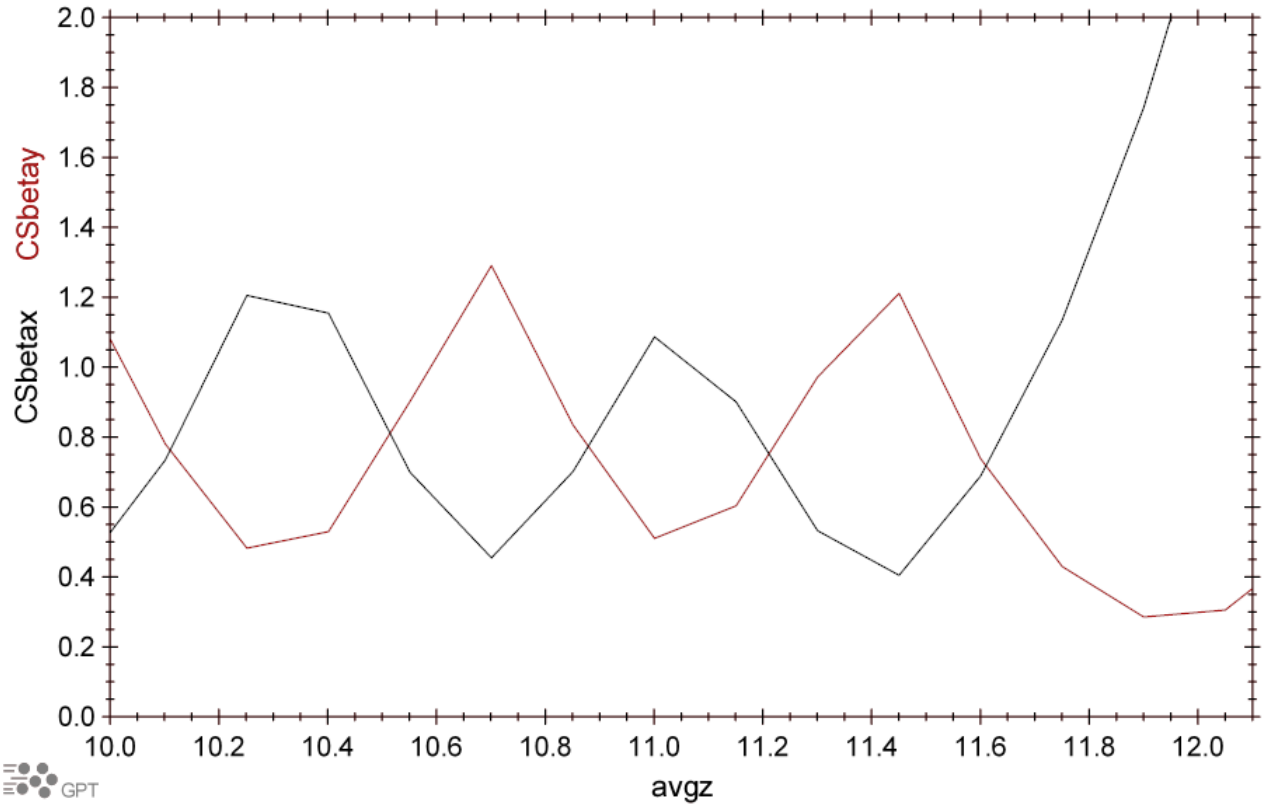

Figure 7: $\beta_{x,y}$ for the tomography section of EMMA injection line at 35 MeV and 0 pC

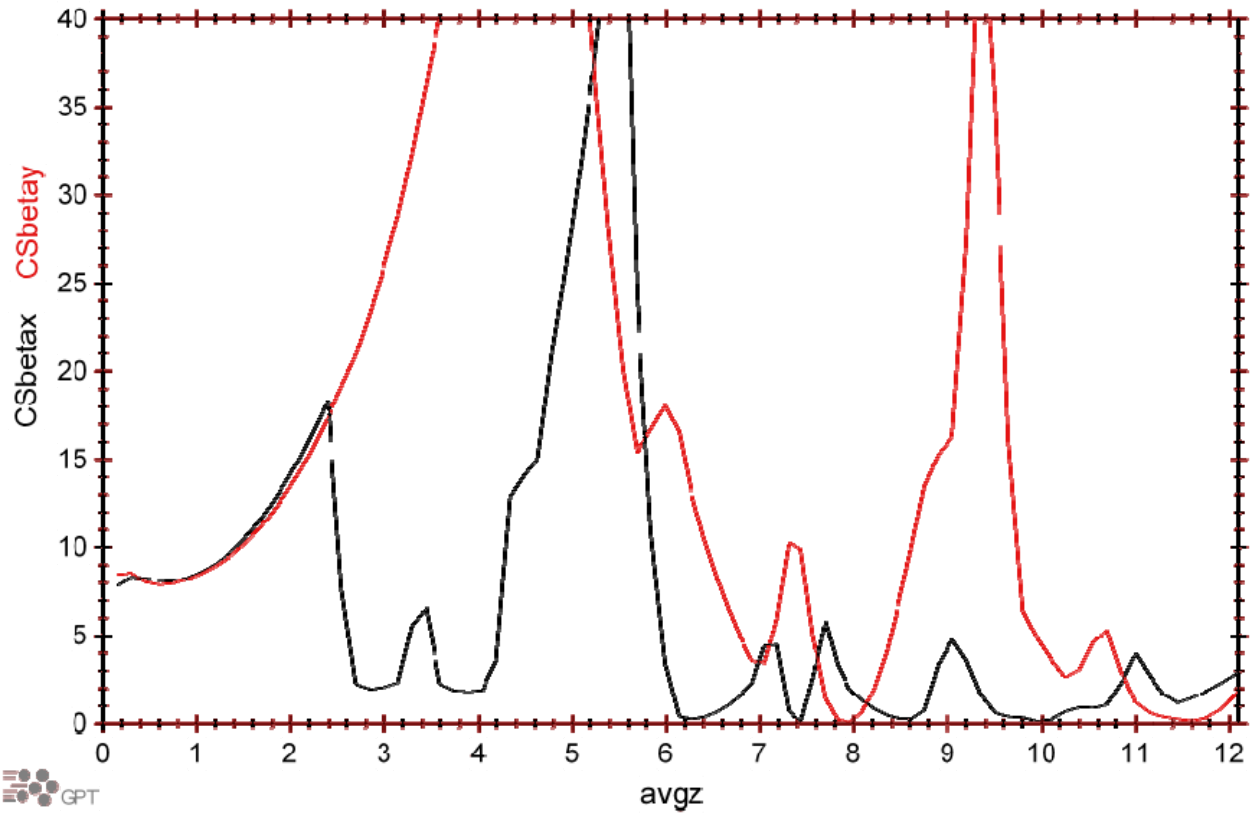

Figure 8: $\beta_{x,y}$ from the ALICE main linac exit to the end of EMMA injection line tomography section at 35 MeV and 80 pC, with no correction for space charge.

The matching is now repeated, at 1, 5, 10, 20, 40 and 80 pC, using as a starting point the quadrupole settings obtained at the previous (lower) bunch charge. Figure 9 shows the beta functions at 80 pC after the effect of space charge has been compensated for by following this procedure. Note the difference in the y-axis scale. Figure 10 is an expansion of the tomography section only. The beta functions from the main linac exit to the first two quadrupoles (at 4.7 m and 5.8 m) grow considerably more for the 80 pC case. If we then look at the tomography section only, we see little difference between figures 7 and 10, suggesting that the combination of 80 pC and 35 MeV is not too difficult for this technique to deal with.

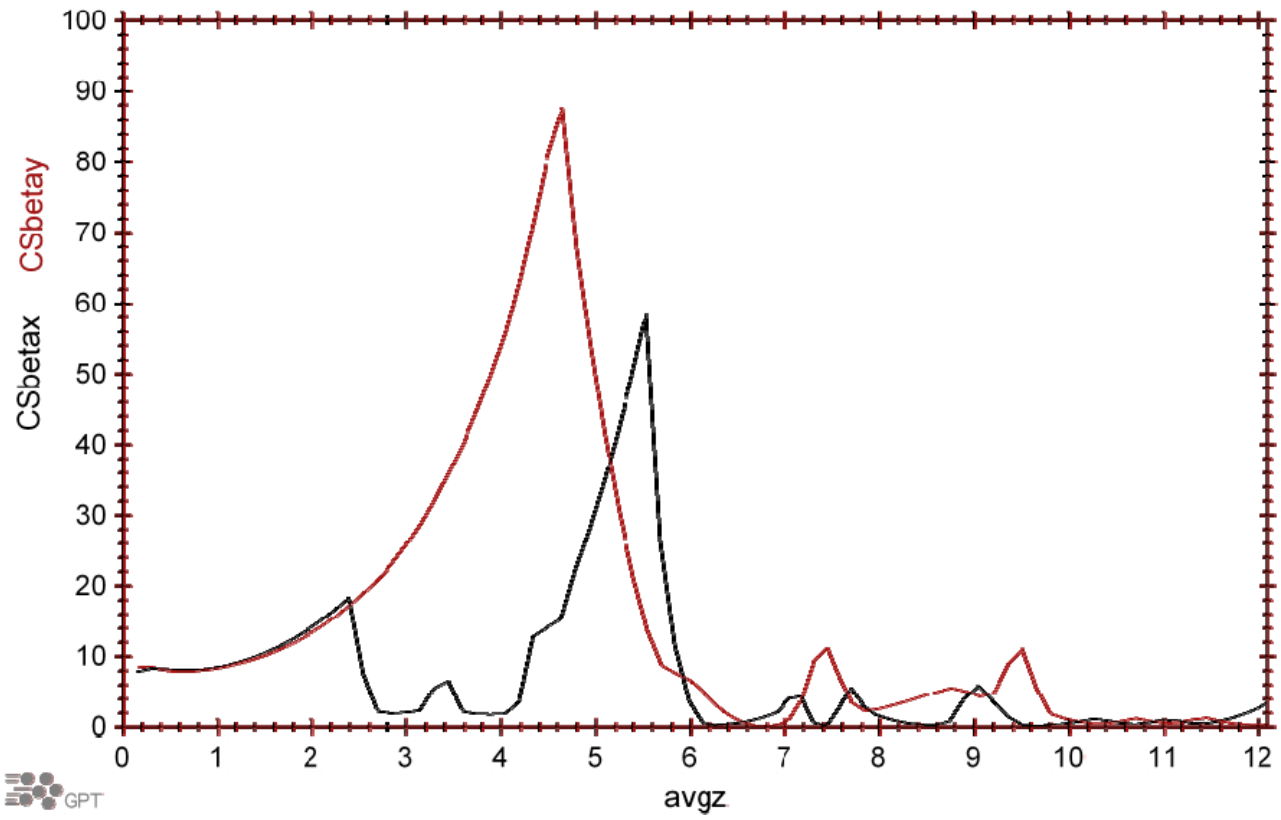

Figure 9: $\beta_{x,y}$ the ALICE main linac exit to the end of EMMA injection line tomography section at 35 MeV and 80 pC, following compensation for space charge

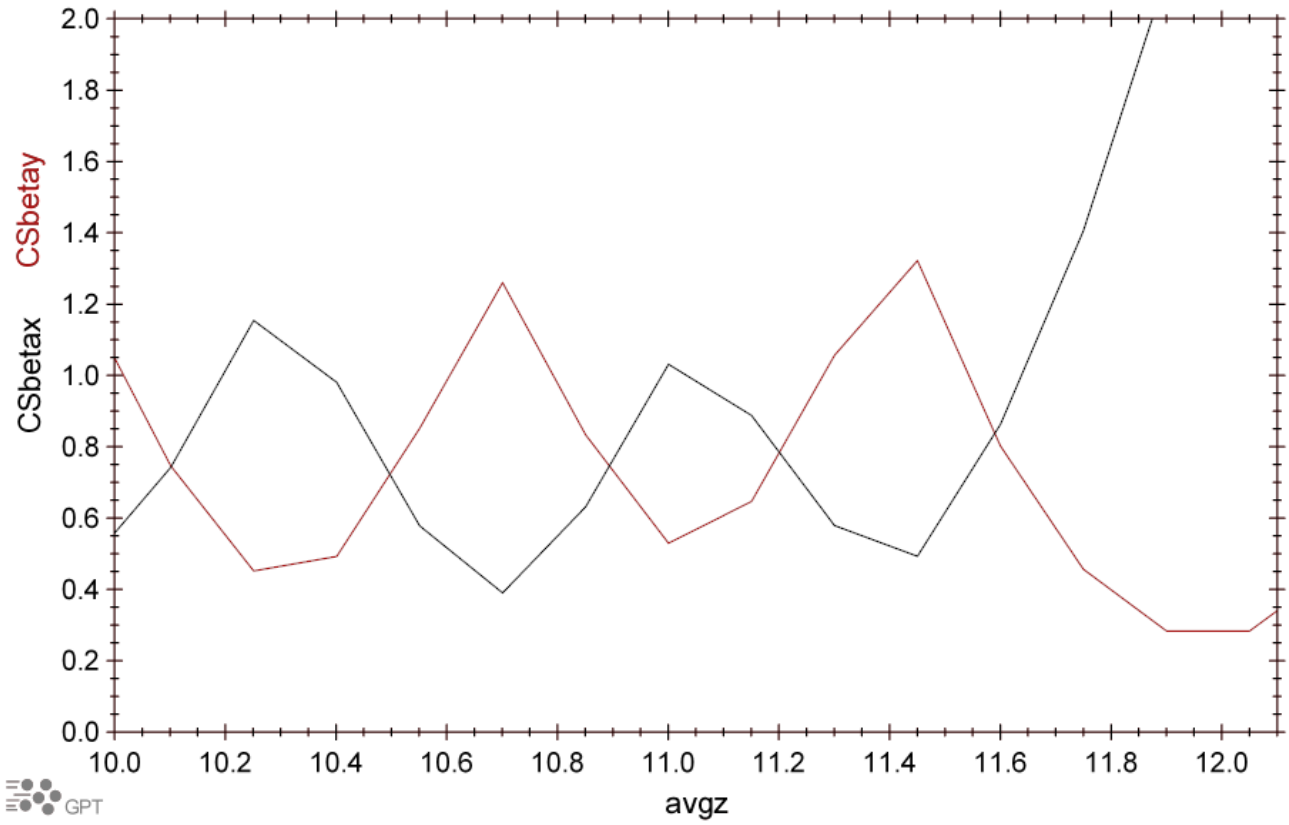

Figure 10: $\beta_{x,y}$ for the tomography section of EMMA injection line at 35 MeV and 80 pC, following compensation for space charge

Table 8 shows the change of the quadrupole strengths required to match the beam into the tomography section as the bunch charge is increased, with figure 11 showing this graphically for ST1-QUAD-01. Clearly, there is not one unique solution (we have more variables than constraints) and MAD and GPT have found significantly different ones.

Table 8: The change of the quadrupole strengths required to match the beam into the tomography section as the bunch charge is increased, calculated in GPT using the "spacecharge3D" routine

Space charge method	**Bunch charge**	**ST1-QUAD-01**	**ST1-QUAD-02**	**EMI-QUAD-04**	**EMI-QUAD-05**	**EMI-QUAD-06**	**EMI-QUAD-07**
		B	**B**	**B**	**B**	**B**	**B**
	(pC)	(T/m)	(T/m)	(T/m)	(T/m)	(T/m)	(T/m)
None (MAD)	-	-0.3113	0.9673	7.148	-5.3182	-3.496	16.04
GPT 3D	0	-0.7405	1.314	5.132	-1.055	-5.779	7.118
GPT 3D	1	-0.7425	1.319	5.140	-1.013	-5.781	7.012
GPT 3D	5	-0.7579	1.328	5.259	-0.980	-5.812	6.972
GPT 3D	10	-0.7689	1.294	5.501	-0.912	-5.869	6.900
GPT 3D	20	-0.7830	1.298	5.527	-0.894	-5.857	6.898
GPT 3D	40	-0.8027	1.325	5.547	-0.875	-5.838	6.904
GPT 3D	80	-0.8162	1.310	5.695	-0.816	-5.844	6.872

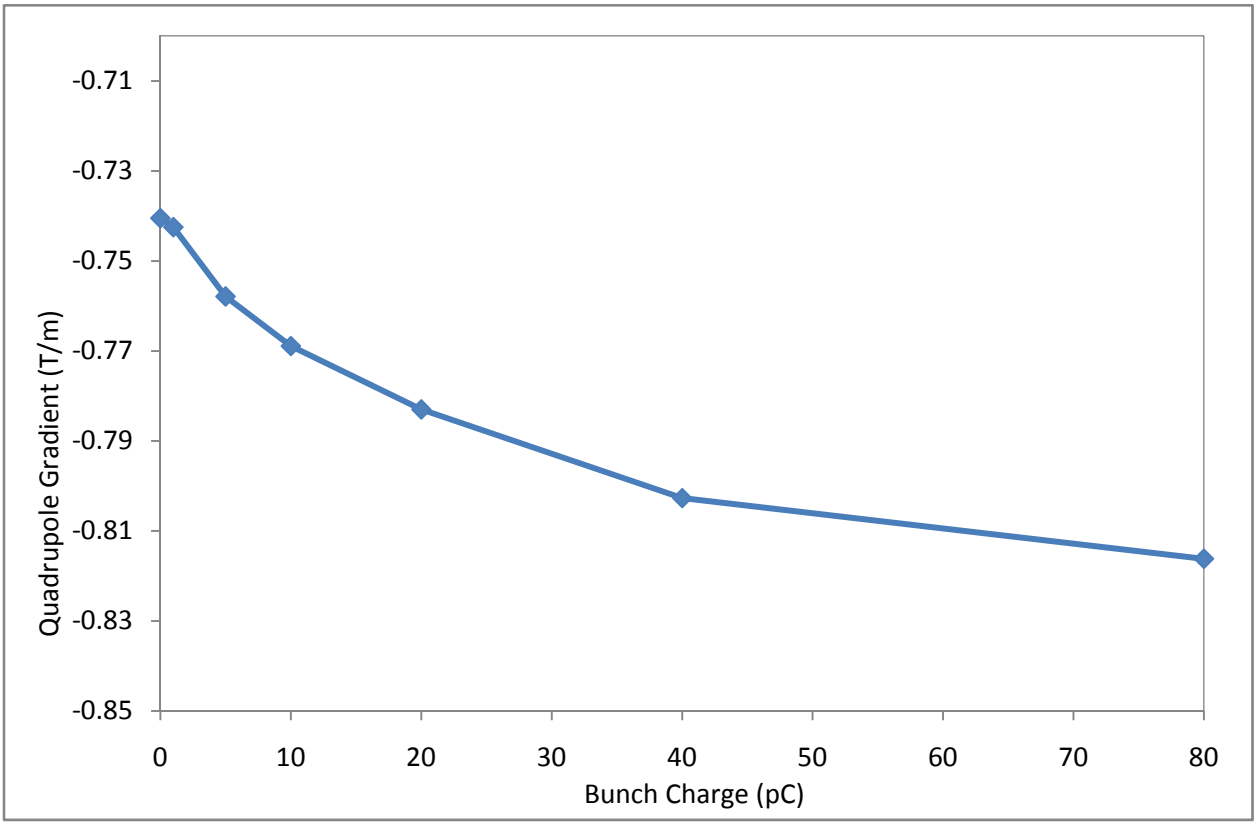

Figure 11: Gradient of quadrupole ST1-QUAD-01 (T/m) (in ALICE prior to the extraction dogleg) at 35 MeV and a range of bunch charges, after using GPT to re-match in the presence of space charge.

FURTHER WORK

There are two unresolved issues with the modelling in MAD, one that can be ignored and one that will need to be dealt with in the future. The first of these is the apparent requirement for quadrupole EMI-QUAD-07 to generate a field greater than the new specification limit. However, you will notice that the setting calculated in GPT, even at its largest, is only 7.1 T/m compared to 16 T/m in MAD and the limit of 14.7 T/m imposed by the magnet and power supply.

Secondly, the Twiss parameters used for MAD modelling at the exit of the booster in ALICE were derived from reference [7], for which ALICE lattice tuning 8.5 was produced. However, more recent work [9] has revised these values following improved simulations of the ALICE injector. A comparison of these two sets of figures can be seen in table 9. Clearly, the more recent result is significantly different, and requires a new ALICE lattice tuning to be produced, which has not been done. Once this has been done, this work can be repeated. However, it is not necessarily true that the Twiss parameters calculated in MAD at the exit of the main linac, which become the starting value for the GPT modelling, will be significantly different.

Table 9: Possible starting Twiss parameters used for MAD modelling

	α_x	α_y	β_x	β_y
			(m)	(m)
Reference [7]	-2.2	-2.2	13.4	13.4
Reference [9]	-5.9	-5.9	39	39

Recent progress with ALICE commissioning has been made at 230 kV/4.8 MeV/20.8 MeV. Clearly therefore, all this work should be repeated under this new regime, where one would expect the effect of space charge

to be greater due to the lower beam energy. An adequate simulation of the injector operating at 230 kV/4.8 MeV does not yet exist, so there are no defensible Twiss parameters for MAD modelling at the exit of the booster linac or emittance value at the exit of the main linac for GPT modelling. Neither is there a new standard ALICE lattice tuning for this regime.

Also, this work should also be repeated with ALICE operating as an EMMA injector, over a range of bunch charges and the intended energy range of 10 to 20 MeV. This work is already underway by another student who will eventually model the whole of EMMA in GPT.

Installation of the EMMA injection line will be completed later this year. In preparation for this, it is intended that an experimental procedure will be developed in order to undertake tomography measurements both for ALICE acting as an EMMA injector and as a stand-alone diagnostic to measure the ALICE beam properties. This will be particularly useful during the FEL commissioning, scheduled to begin in September 2009.

CONCLUSION

The feasibility of converting the EMMA injection line into a useful diagnostic for measuring the properties of the full-energy ALICE beam was assessed and a number of hardware changes specified. These are primarily the addition of OTR screens in parallel to the existing YAG screens and increasing the maximum current limit of the magnet power supplies. Fortunately it was not necessary to change any of the existing magnets.

Furthermore, the effect of space charge in the EMMA injection line, on the matching of the electron beam into the tomography diagnostic, has been calculated at 35 MeV with 80 pC bunches. A technique to compensate for the effect of space charge has been demonstrated, which involves using the code GPT to progressively re-calculate the matching as the bunch charge is increased from zero to the desired value. With this combination of energy and bunch charge it has been possible to apparently eliminate the effect of space charge almost entirely at the start of the tomography section.

APPENDICES

Appendix 1: EMMA injection line dipole parameters					
Energy	20		35		MeV
Type	F	G	F	G	
Magnetic length	202	202			mm
Yoke length	182	182			mm
Bend angle	30	33			°
Bend radius	386	352			mm
Field	0.173	0.190	0.303	0.333	T
Pole width	198	170			mm
Gap	50	40			mm
Ampere turns per pole +5%	3543	3125	6200	5470	At
Conductor width or diameter	1.2	1.2			mm
Conductor height	6.5	6.5			mm
Conductor cross sectional area	7.585	7.585			mm^2
Current density	0.794	0.701	1.39	1.23	A/mm^2
Copper cross sectional area per coil	4460	6525			mm^2
Number of turns per coil	588	588			turns
Current per turn	6.03	5.32	10.5	9.30	A
Coil Across	28	28			
Coil Down	21	21			
Coil Width	45	45			mm
Coil Height	145	145			mm
Minimum coil bend radius	15	15			mm
Conductor length per magnet	1167	1098			m
Resistance per magnet at 20°C	2.58	2.43			Ω
Resistance per coil at 20°C	1.29	1.21			Ω
Resistance per magnet at 40°C	2.79	2.62			Ω
Circuit resistance	2.79	7.87			Ω
Volts per magnet	16.8	14.0	29.4	24.4	V
Volts per coil	8.4	7.0	14.7	12.2	V
Power per magnet	101	74	310	227	W
Power per coil	51	37	155	114	W

Appendix 2: EMMA injection line quadrupole parameters					
Energy	20		35		MeV
Type	G	H	G	H	
Magnetic length	0.310	70			mm
Field gradient G	1.4	8.5	2.4	14.7	T/m
K1	20	124			m^{-2}
Integrated gradient		0.60		1.0	T
Pole width		50			mm
Inscribed radius	35	20			mm
Yoke length	0.304	50			mm
Ampere turns per pole IN +5%		1459		2553	At
Conductor size X		1.4			mm
Conductor size Y		2.8			mm
Conductor cross sectional area		3.9			mm^2
Conductor current density		1.4		2.5	A/mm^2
Copper cross sectional area per coil		1015			mm^2
Number of turns		259			turns
Current	66	5.6	115	10	A
Coil across		7.0			
Coil down		37.0			
Coil width		9.8			mm
Coil height		103.6			mm
Minimum coil bend radius		5			mm
Conductor length per magnet		327			m
Resistance per magnet at 20°C		1.40			Ω
Resistance per coil at 20°C		0.35			Ω
Resistance per magnet at 40°C	0.015	1.51			Ω
Maximum voltage per magnet	1.0	8.5	1.7	14.9	V
Voltage per coil		2.1		3.7	V
Power per magnet		48		147	W
Power per coil		12.0		36.7	W

REFERENCES

[1] Y.M.Saveliev et al, "Results from ALICE (ERLP) DC Photoinjector Gun Commissioning", EPAC'08, Genoa, July 2008.

[2] S.L.Smith et al, "Progress on the Commissioning of ALICE, the Energy Recovery Linac-Based Light Source at Daresbury Laboratory", PAC'09, Vancouver, May 2008.

[3] S.L.Smith et al, "EMMA, the World's First Non-Scaling FFAG Accelerator", PAC'09, Vancouver, May 2008.

[4] B.D.Muratori et al, "Injection and Extraction for the EMMA NS-FFAG", EPAC'08, Genoa, July 2008.

[5] B.D.Muratori et al, "Matching with Space Charge", EPAC'08, Genoa, July 2008.

[6] GPT (General Particle Tracer), www.pulsar.nl/gpt/

[7] C.K.M.Gerth, F.E. Hannon, "Injector Design for the 4GLS Energy Recovery Linac Prototype", EPAC'04, Lucerne, July 2004.

[8] B.D.Muratori et al, "Beam Dynamics Simulations through Diagnostic Devices", EUROFEL-Report-2007-DS1-059a.

[9] B.D.Muratori, Y.M.Saveliev, "ALICE (ERLP) Injector Design", EPAC'08, Genoa, July 2008.

[10] K. Flötmann, ASTRA (A Space charge TRAking code) User Manual, http://www.desy.de/~mpyflo/.

[11] B.D.Muratori et al, "Space Charge Effects for the ERL Prototype at Daresbury Laboratory", EPAC'04, Lucerne, July 2004.